Effect of Pressure on the Dynamic Heterogeneity in Miscible Blends of Poly(methyl methacrylate) with Poly(ethylene oxide)

K. Mpoukouvalas and G. Floudas*

Department of Physics, University of Ioannina, P.O. Box 1186, 451 10 Ioannina, Greece, and Foundation for Research and Technology-Hellas (FORTH), Biomedical Research Institute (BRI)

Received October 16, 2007; Revised Manuscript Received December 19, 2007

ABSTRACT: The poly(methyl methacrylate) (PMMA) segmental dynamics in miscible blends of PMMA with poly(ethylene oxide) (PEO) were studied as a function of pressure by means of dielectric spectroscopy (DS). This facilitates a test of the predictions of the self-concentration model proposed by Lodge and McLeish, at elevated pressures. We find that pressure increases the glass temperature and slows down the segmental dynamics but does not affect the length scale or the self-concentration associated with the dynamic glass transition. This is in agreement with the expectations borne out from the model.

Introduction

The dynamics in miscible polymer blends are far more rich than originally anticipated. The components, despite being thermodynamically mixed, can exhibit distinct dynamic behavior, known as dynamic heterogeneity.[1−7] This dynamic heterogeneity, which has been found also in polymer/solvent mixtures,[8,9] manifests itself by (i) the two segmental processes with different temperature dependences, (ii) the broadening of the relaxation spectra, and (iii) the breakdown of the time−temperature superposition.[1,5] Different models have been proposed to account for the distinct component dynamics that emphasize either *intermolecular* concentration effects through the concentration fluctuation approach[10] or *intramolecular* effects through the chain connectivity[11] or various combinations of both.[12−18]

PMMA/PEO is by far the most studied miscible blend: rheology,[1] differential scanning calorimetry (DSC),[19−23] pressure−volume−temperature (PVT) measurements,[24,25] Brillouin scattering,[26] neutron scattering,[27−30] computer simulations,[30] deuterium NMR,[31] forced Rayleigh scattering,[32] and dielectric spectroscopy (DS)[23] are the main techniques that have been employed in the study of the thermodynamic state and of the dynamic heterogeneity at the segmental and chain length scales. There are two main features that made this system so popular. First, the fact that it remains miscible over the whole composition range, provided that PEO stays in the melt state (above the crystallization temperature or, better, above the equilibrium melting temperature of PEO). There is some disagreement in the literature with respect to the exact phase state which reflects the very small value of the interaction parameter χ.[33−36] The second feature is the very large difference between the component glass temperatures ($\Delta T_g \sim 180$ K), which exemplifies the dynamic heterogeneity.

From these studies some additional features emerged. In one such study[31] the PEO segmental dynamics were found to be hardly influenced by the presence of the slow-moving PMMA (being up to 12 orders of magnitude faster than the PMMA segmental dynamics). In addition, different studies reported contradictory results in explaining the PMMA and PEO segmental blend dynamics, based on a model that emphasizes intramolecular effects.[6,27,29]

Herein, we employ the same blend system PMMA/PEO as well as the homopolymers and study the PMMA segmental dynamics in the blends rich in PMMA, for the first time, as a function of pressure. The homopolymer investigation provides essential information on the origin of the liquid-to-glass transition that is used as an input to the blend study. The blend study provides a critical test of the self-concentration ideas put forward by Lodge and McLeish (LM).[11] According to these ideas, the origin of the distinctly different component dynamics in miscible blends is the intramolecular connectivity that bias the local concentration to values away from the average blend composition. LM proposed that the relevant length scale for evaluating the self-concentration is of the order of the Kuhn segment, l_K. As such, the length scale is polymer specific, independent of blend composition, and only weakly dependent on the other thermodynamic variables of temperature (T) and pressure (P).

Instead of using different methods with different sensitivities, we employ dielectric spectroscopy—a technique well-known for its sensitivity toward local environments—and a series of PMMA/PEO miscible blends and investigate the PMMA segmental dynamics at elevated pressures. In this way we address the following straightforward question: given the small variation of the Kuhn length and of the corresponding self-concentration with pressure, *can the PMMA segmental dynamics in the blends described equally well at atmospheric and at elevated pressures? If not, how strong is the pressure dependence that we need to invoke*? A strong pressure dependence would be against the predictions of the LM model.

Experimental Section

Samples. The PMMA ($M_w = 21\,400$ g/mol and polydispersity index, $M_w/M_n = 1.07$) and PEO ($M_w = 17\,300$ g/mol, $M_w/M_n = 1.05$) used in the present study were purchased from Polymer Source Inc. Molecular weights were determined by size exclusion chromatography in THF. The PMMA sample was 79% syndiotactic based on ^{1}H NMR. Blends of PMMA/PEO were made by dissolving both polymers in a 95% w/w $CHCl_3$. Solutions were stirred for more than 6 h, and the solvent was slowly removed by evaporation at ambient temperature. Uniform bubble-free films were prepared by drying in a desiccator at 373 K for 1 week. Traces of solvent were further removed by drying under vacuum at 373 K.

Differential Scanning Calorimetry (DSC). A Mettler Toledo Star DSC was employed with a cooling/heating rate of 10 K/min.

* Corresponding author. E-mail: gfloudas@cc.uoi.gr.

10.1021/ma702299n CCC: $40.75
Published on Web 01/30/2008

Two heating/cooling circles were made, and the reported glass temperatures correspond to the second cooling circle. Two glass temperatures were evident for the blends with $0.5 < \varphi_{PMMA} < 0.9$. All DSC glass temperatures are discussed with respect to Figure 4. PEO crystallized in the blends with $\varphi_{PMMA} = 0.2$ (with a heat of fusion, $\Delta H = 120$ J/g), $\varphi_{PMMA} = 0.4$ ($\Delta H \sim 25$ J/g), and $\varphi_{PMMA} = 0.5$ ($\Delta H = 48$ J/g) and only weakly in $\varphi_{PMMA} = 0.6$ ($\Delta H \sim 7$ J/g). These results were confirmed by independent wide-angle X-ray (WAXS) measurements (not shown here). The WAXS profiles for the blends with $\varphi_{PMMA} < 0.6$ contained the usual Bragg reflections characteristic of the monoclinic unit cell of PEO. In contrast, in the PMMA-rich blends these intense reflections were absent, revealing the complete suppression of PEO crystallization. Since PEO crystallization drives phase demixing in the blends, herein we will only discuss blends rich in PMMA (i.e., $\varphi_{PMMA} > 0.6$).

Dielectric Spectroscopy (DS). The complex dielectric permittivity $\epsilon^* = \epsilon' - i\epsilon''$, where ϵ' is the real and ϵ'' is the imaginary part, is a function of frequency ω, temperature T, and pressure P, $\epsilon^* = \epsilon^*(\omega,T,P)$. For that reason the dielectric measurements were made under both "isobaric" and "isothermal" conditions. (In reality, all measurements are made under isobaric *and* isothermal conditions, but we use these terms here to indicate a series of measurements made by increasing temperature while keeping the pressure constant or by increasing pressure while keeping the temperature constant.) The "isobaric" measurements were made at different temperatures in the range 123.15−503.15 K, at atmospheric pressure, whereas the "isothermal" measurements were made for pressures up to 300 MPa for a range of temperatures. In both cases the frequency range was from 3×10^{-3} to 1×10^6 Hz as set by a Novocontrol BDS system composed from a frequency response analyzer (Solartron Schlumberger FRA 1260) and a broadband dielectric converter. The sample cell consisted of two electrodes with 20 mm in diameter and the sample with a thickness of 50 μm. The setup for the pressure-dependent DS measurements consisted of a temperature-controlled sample cell, a hydrostatic closing press with pump, and a pump for hydrostatic test pressure.[37] Silicon oil was used as the pressure transducing medium. The sample capacitor was sealed and placed inside a Teflon ring to separate the sample from the silicon oil. Figure 1 gives some representative loss spectra for the PMMA homopolymer under "isobaric" (at 0.1 MPa) and "isothermal" (at 481.15 K) conditions. Notice that decreasing T and increasing P results in the separation of the merged $\alpha\beta$-process at higher T to two processes (α and β). In the analysis of the DS spectra we have used a summation of two Havriliak and Negami (HN)[38] equations

$$\frac{\epsilon^*(T,P,\omega) - \epsilon_\infty(T,P)}{\Delta\epsilon(T,P)} = \frac{1}{[1 + (i\omega\tau_{HN}(T,P))^m]^n} \quad (1)$$

where $\tau_{HN}(T,P)$ is the characteristic relaxation time in this equation, $\Delta\epsilon(T,P) = \epsilon_0(T,P) - \epsilon_\infty(T,P)$ is the relaxation strength of the process under investigation, and m, n (with limits $0 < m, mn \leq 1$) describe respectively the symmetrical and asymmetrical broadening of the distribution of relaxation times. In the fitting procedure we have used the ϵ'' values at every temperature, and in some cases the ϵ' data were also used as a consistency check. The linear rise of the ϵ'' at lower frequencies is caused by the conductivity ($\epsilon'' \sim (\sigma_0/\epsilon_f)\omega^{-1}$, where σ_0 is the dc conductivity and ϵ_f is the permittivity of free space) which has been included in the fitting procedure. From τ_{HN}, the relaxation time at maximum loss, τ_{max}, is obtained analytically following

$$\left[\sin\left(\frac{\pi m}{2+2n}\right)\right]^{1/m} \tau_{max} = \tau_{HN}\left[\sin\left(\frac{\pi mn}{2+2n}\right)\right]^{1/m} \quad (2)$$

For the neat PMMA and the blends there is a strong conductivity contribution. In these cases we have used the first derivative method of ϵ' to derive the ϵ'' as $\epsilon''_{calc} = -(\pi/2)(\partial\epsilon'/\partial \ln \omega)$, which provides an ohmic conduction-free dielectric loss. In an alternative approach, the electric modulus (M^*) representation can be employed, related to the dielectric permittivity ϵ^* through $M^*(T,P,\omega) = 1/\epsilon^*(T,P,\omega)$.[39]

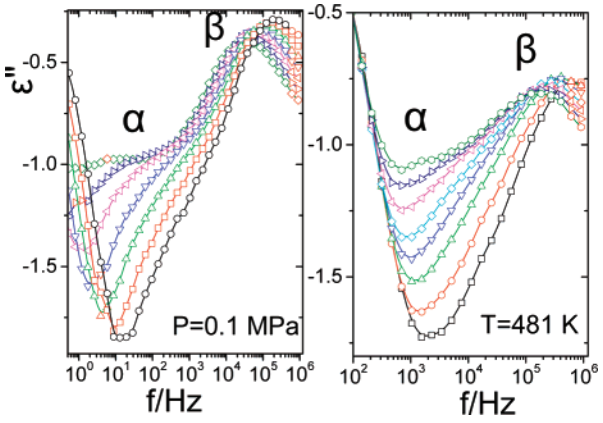

Figure 1. Dielectric loss curves for PMMA under "isobaric" (P = 0.1 MPa) (left) and "isothermal" conditions (T = 481.15 K). The isobaric curves are at (circles) 427.15 K, (squares) 423.15 K, (up triangles) 419.15 K, (down triangles) 415.15 K, (left triangles) 411.15 K, (right triangles) 407.15 K, and (rhombus) 403.15 K and the isothermal curves at (squares) 120 MPa, (circles) 140 MPa, (up triangles) 160 MPa, (down triangles) 180 MPa, (rhombus) 200 MPa, (left triangles) 220 MPa, (right triangles) 240 MPa, and (polygons) 260 MPa. The Greek letters α and β indicate respectively the segmental and local processes of PMMA.

The relaxation times thus obtained (τ_{M^*}) may differ from the corresponding τ_{ϵ^*} times, depending on the strength of the process under investigation as $\tau_{M^*}/\tau_{\epsilon^*} \sim \epsilon_\infty/\epsilon_0$. In our analysis we have employed both representation but the reported times are from the ϵ^* representation.

Results and Discussion

PMMA Dynamics. The homopolymer dynamics where investigated as a function of T and P. Decreasing T/increasing P results in the separation of the mixed $\alpha\beta$-process to two (α and β) well-separated processes (Figure 1). Two HN functions together with the ionic contribution were used in this case. The two processes display distinctly different $\tau(T)$ dependencies. The slower α-process (with shape parameters $m = 0.47$, $mn = 0.15$) follows the well-known Vogel−Fulcher−Tammann (VFT) equation

$$\tau_{max} = \tau_0 \exp\left(\frac{B}{T - T_0}\right) \quad (3)$$

where B (= 1056 K) is the activation parameter, τ_0 (= 8×10^{-12} s) the relaxation time in the limit of very high temperatures, and T_0 (= 358 K) the "ideal" glass temperature. In contrast, the β-process has an Arrhenius T dependence

$$\tau_{max} = \tau_0 \exp\left(\frac{E}{k_B T}\right) \quad (4)$$

with an activation energy $E = 80$ kJ/mol. Herein we are mainly interested in the dynamic heterogeneity in the miscible blends of PMMA with PEO and thus will concentrate on the α-process that is actually probing the heterogeneity.

The origin of the α-process and the associated freezing of the segmental dynamics at the liquid-to-glass "transition" is one of the fundamental problems in polymer physics.[40] Two extreme cases consider (i) thermally activated processes on a constant-density energy landscape[41,42] and (ii) free-volume arguments.[43] In the former picture, the controlling parameter is temperature, the landscape is considered as fixed, and the strong $\tau(T)$ is attributed to changes in the barriers and the minima encountered in the exploration of the landscape. In the latter picture, the controlling parameter is volume (V) or density (ρ) and the

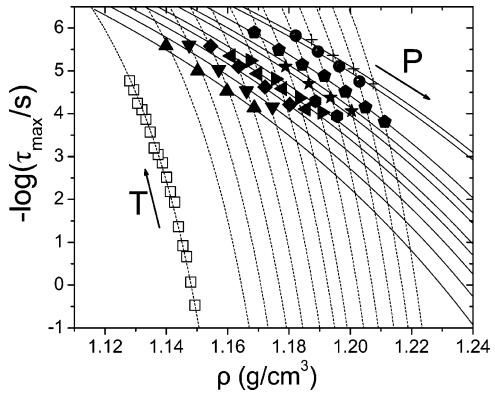

Figure 2. Relaxation times for the PMMA segmental (α) process plotted as a function of density. The open symbols correspond to the data measured "isobarically" (at $P = 0.1$ MPa), and the filled symbols correspond to data measured "isothermally" at different temperatures: (up triangles) 446.15 K, (down triangles) 451.15 K, (rhombus) 456.15 K, (left triangles) 461.15 K, (right triangles) 466.15 K, (polygons) 471.15 K, (stars) 476.15 K, (pentagons) 481.15 K, (spheres) 486.15 K, and (crosses) 491.15 K. The solid and dashed lines represent VFT fits to the "isothermal" and "isobaric" data, respectively.

slowing down results from the decrease of the available or "free" volume. Since changing T affects both the thermal energy (k_BT) and the density, it is impossible to separate the two effects by T variation alone. To this end, pressure-dependent measurements have been of paramount importance since pressure can be applied isothermally (affecting only ρ) and hence have been employed in a number of systems (both polymers and molecular glass-formers) to separate the two effects.[39,44−49]

Of central importance in discussing the origin of the liquid-to-glass transition is the dynamic quantity, E_V^*/H^*, i.e., the ratio of the activation energy at constant volume $E_V^* = R(\partial \ln \tau/\partial(1/T))_V$, to the enthalpy of activation $H^* = R(\partial \ln \tau/\partial(1/T))_P$.[44,50] This ratio assumes values in the range 1−0 and provides a quantitative measure of the role of temperature and density on the dynamics. Values near one suggest that the dynamics are governed mainly by the thermal energy, whereas values near zero suggest that the free volume ideas prevail, since in this case, $E_V^* = 0$. However, there is not a single polymer or glass-forming liquid with values of 0 or 1, suggesting that the picture is more complicated than the two extreme cases considered above. Experimentally this ratio can be obtained from either thermodynamic[46] or dynamic means, as for example[44,50]

$$\frac{E_V^*}{H^*} = 1 - \left(\frac{\partial P}{\partial T}\right)_V \left(\frac{\partial T}{\partial P}\right)_\tau \tag{5}$$

or from the from the $\tau(\rho)$ representation as[39]

$$\frac{E_V^*}{H^*} = 1 - \frac{\left(\frac{\partial \ln \tau}{\partial \rho}\right)_T}{\left(\frac{\partial \ln \tau}{\partial \rho}\right)_P} \tag{6}$$

This is made by coupling the relaxation times measured under "isobaric" $\tau(T)$ and "isothermal" $\tau(P)$ conditions with independent measurements of the equation of state $V(T,P)$. The result for PMMA is shown schematically in Figure 2. The solid and dashed lines represent the "isothermal" and "isobaric" pathways in the $\tau(\rho)$ representation, and the lines are fits to the modified VFT equation for the density representation. The ratio E_V^*/H^* is then obtained directly (from eq 6) at the crossings of the "isotherms" and "isobars", and its P and T dependence is depicted in Figure 3.

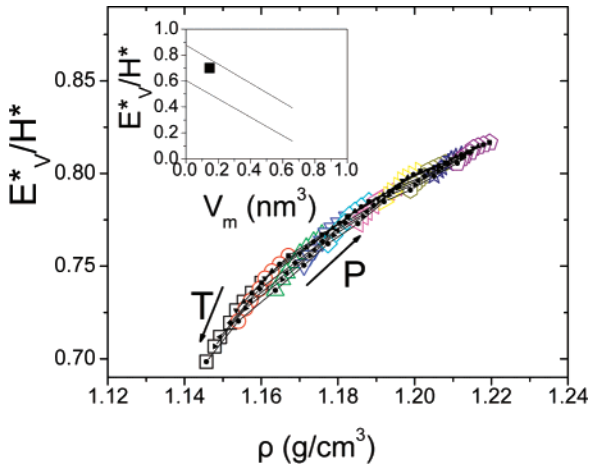

Figure 3. Ratio of activation energies under constant volume and under constant pressure plotted against density for different temperatures and pressures corresponding to the crossings of the "isothermal" and "isobaric" curves of Figure 2. In the inset the value of the ratio of activation energies for PMMA at T_g is plotted as a function of the monomer volume. The lines give the range within which many polymers and glass-forming liquids lie.[51]

Recently, it has been demonstrated[51] that monomer volume and local packing play a key role in controlling this ratio and thus the dynamics of glass-forming systems near T_g. This was documented by plotting the dynamic ratio, E_V^*/H^*, as a function of the monomer volume for a number of polymers and glass-forming liquids. It was shown that in flexible main-chain polymers the dynamics are controlled mainly by the intramolecular barriers, whereas in polymers with bulky side groups and large monomer volumes, density and intermolecular correlations gain importance. Similarly, the explanation of the higher values of the dynamic ratio E_V^*/H^* of molecular glass-formers is their larger volume and irregular shape that is required to prevent them from crystallizing. The PMMA studied herein fits nicely to these ideas. The calculated value of $E_V^*/H^* \sim 0.7$ (at $T = T_g$ and at $P = 0.1$ MPa) is located well within the expected range and is plotted in the inset to Figure 3. This value is in agreement with a recent independent study on bulk PMMA.[52]

These results have also consequences with respect to the issue of dynamic heterogeneity in polymer blends and copolymers;[53−55] the appropriate choice of monomers could result in drastically different T and P dependencies for the two components, with consequences on their dynamic response and possibly their thermodynamic miscibility. As an example we refer to the athermal poly(isoprene-*b*-vinylethylene) (PI-*b*-PVE) melt.[53] It has been shown that pressure, unlike temperature, induces dynamic heterogeneity through the different pressure sensitivity of the two homopolymers.

Blend Dynamics. The pressure-dependent investigation of bulk PMMA, and more specifically the high value of the activation ratio, E_V^*/H^*, suggests that the segmental dynamics are largely determined by the intramolecular barriers. This higher sensitivity of the segmental dynamics to intramolecular conformational changes is due to the relatively small monomer volume of MMA.[51] Therefore, in discussing the PMMA segmental dynamics in its blends with PEO, we need models that emphasize *intramolecular* correlations and *nondiverging* length scales, the latter of the monomer size or so. This of course is not to say that intermolecular effects are unimportant. If that was the case, then the ratio of activation energies would be close to unity, which is never the case for glass-forming systems. The

expectation borne out from our earlier study[51] is that for polymers with bulky side groups and larger repeat volumes (like, i.e., bis-phenol-A-polycarbonate[49]) intermolecular effects would play a dominant role in the segmental dynamics. Therefore, in miscible blends comprising such components, intermolecular effects and the associated concentration fluctuations may play the dominant role. However, because the liquid-to-glass transition in PMMA is driven mainly by intramolecular effects, it suffices to a good approximation to employ only such effects in discussing the PMMA segmental dynamics in the blends.

The model that has these ingredients, i.e., intramolecular effects and nondiverging length scales, is the recently proposed "self-concentration" model of Lodge and McLeish (LM).[11] According to the model, the average composition of the local environment around any chosen segment is enriched in the same species because of chain connectivity effects (correlation hole effect). Because of this, each species will experience a different average local environment, and to the extent that the glass transition is sensitive to composition, each polymer will sense its own composition-dependent glass temperature. In a binary blend of homopolymers A and B, the effective local concentration is defined by

$$\varphi_{\mathrm{eff},i} = \varphi_{\mathrm{S},i} + (1 - \varphi_{\mathrm{S},i})\langle\varphi\rangle \tag{7}$$

where i represents component A or B, φ_S is the self-concentration, and $\langle\varphi\rangle$ is the average blend composition. According to the LM model,[11] the relevant length scale in evaluating the self-concentration is the Kuhn length (l_K) of the polymer. This is a reasonable approximation since l_K is an intramolecular length scale (associated with the extent of backbone conformational transitions), independent from blend composition and only weakly dependent on T and P variations. Then the self-concentration is determined from the volume fraction occupied by monomers in one Kuhn length inside a volume $V = l_K^3$ as

$$\varphi_S = \frac{C_\infty M_0}{k\rho N_A V_K} \tag{8}$$

where C_∞ is the characteristic ratio, M_0 is the repeat unit molar mass, N_A is the Avogadro number, and k is the number of backbone bonds per repeat unit. The model associates the average local concentration of each component with a local glass temperature

$$T_{g,\mathrm{eff}} = T_g(\varphi)|_{\varphi=\varphi_{\mathrm{eff}}} \tag{9}$$

Hence, the effective glass temperature $T_{g,eff}$ is determined from the macroscopic $T_g(\varphi)$ but evaluated at φ_{eff} rather than φ. For the macroscopic composition dependence of the glass temperature the well-known Fox equation was assumed but with the effective concentration for each component instead of the total blend composition $\langle\varphi\rangle$ as

$$\frac{1}{T_g(\varphi)} = \frac{\varphi_A}{T_{g,A}} + \frac{1-\varphi_A}{T_{g,B}} \tag{10}$$

In Figure 4 we plot the measured glass temperatures from DSC and DS (defined at $\tau \sim 1$ s) for the PMMA and PEO components as a function of PMMA composition (φ_{PMMA}). The thick solid line is the prediction of the usual Fox equation, whereas the corresponding model predictions using eq 9 for the PMMA and PEO glass temperatures are shown, respectively, with the thinner solid lines. In the calculation we have used $C_\infty = 9$,[11] $M_0 = 0.100$ kg/mol, $k = 2$, $\rho = 1130$ kg/m^3, $l_K = 1.38$ nm resulting in $\varphi_S = 0.25$ for PMMA and $C_\infty = 5.5$,[56] $M_0 = 0.044$ kg/mol, $k = 2$, $\rho = 1212$ kg/m^3, $l_K = 0.81$ nm, and $\varphi_S = 0.21$ for PEO. Clearly, the self-concentration model predictions for the PMMA segmental dynamics in the blends provide an adequate description of the experimental data without using any adjustable parameter. On the other hand, the model predictions fail for PEO, but this is due to the PEO crystallization in the PEO-rich blends that locally enriches the PEO component and drives the system to phase separation. Therefore, in the remaining we discuss the PMMA segmental dynamics by focusing in the temperature range where the system is in a thermodynamically mixed state. If, on the other hand, we allow for the characteristic length scale to be an adjustable parameter and fit the DS glass temperatures, a better agreement is reached, with $\varphi_S = 0.16$ corresponding to $l_K = 1.62$ nm, i.e., with a value of about 15% higher than the theoretical value. We mention here that a recent calorimetric study[19] of PMMA/PEO blends comprising a low molecular weight PEO ($M_n = 300$ g/mol), which was unable to crystallize, resulted in a higher φ_S (=0.60). We are not sure about the origin of this difference, but it could reflect the different sensitivity of DS with respect to DSC.

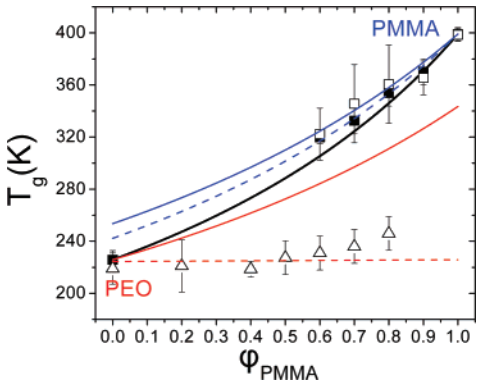

Figure 4. Glass temperature obtained from DSC (open symbols) and DS (filled symbols) plotted as a function of PMMA concentration. The PMMA and PEO glass temperatures are indicated with squares and triangles, respectively. The black line is the prediction of the Fox equation. The predictions of the self-concentration model for the PMMA ($l_K = 1.38$ nm) and PEO ($l_K = 0.81$ nm) segmental dynamics are given by the solid lines. The dashed line for the high-T_g component (PMMA) is the result of a fit to the DS data through the self-concentration model but now using l_K as a free parameter ($l_K^* = 1.62$ nm). The dashed line for the low-T_g component (PEO) indicated a $l_K^* = 0.48$ nm corresponding to $\varphi_s = 1$.

So far, the model predictions were tested for the dynamic (DS) T_g, but at a single relaxation time of ~1 s. In Figure 5 we test the model predictions against the full $\tau(T)$ dependence at 0.1 MPa. Only the PMMA segmental dynamics are shown, which have been separated from the local β-process as described in the Experimental Section. The two Arrhenius relaxation maps display the same relaxation times for the PMMA, PEO homopolymers, and four PMMA/PEO blends rich in PMMA against the LM model predictions using the theoretical Kuhn length ($l_K = 1.38$ nm) or the adjustable length ($l_K = 1.62$ nm). In doing so, we have used the following VFT parameters: $B = 1056$ K, $\tau_0 = 8 \times 10^{-12}$ s, and $T_0 = 358$ K for PMMA and $B = 3570$ K, $\tau_0 = 1 \times 10^{-14}$ s, and $T_0 = 115$ K for PEO. For the PMMA segmental dynamics in the blends we have further assumed[6]

$$\tau_i(\varphi_{\mathrm{eff}}, T) = \tau_{0,i} \exp\left(\frac{B_i}{T - T_{0,i}(\varphi_{\mathrm{eff}})}\right) \tag{11}$$

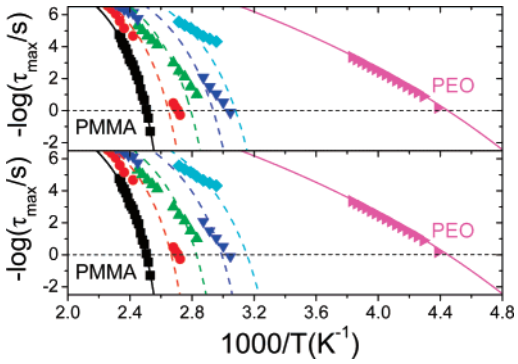

Figure 5. Arrhenius relaxation map of the segmental dynamics in the homopolymers ((squares) PMMA, (right triangles) PEO) and the PMMA/PEO blends with $\varphi_{PMMA} = 0.9$ (circles), $\varphi_{PMMA} = 0.8$ (up triangles), $\varphi_{PMMA} = 0.7$ (down triangles), and $\varphi_{PMMA} = 0.6$ (rhombus). The solid lines represent VFT fits to the homopolymer relaxation times. The dashed lines are also VFT fits to the PMMA dynamics in the PMMA/PEO blends using the self-concentration model either with the theoretical l_K (=1.38 nm) (top) or the adjustable l_K (=1.62 nm) (bottom). The horizontal dashed lines correspond to a segmental relaxation time of $\tau \sim 1$ s.

with identical B_i and $\tau_{0,i}$ parameters as for bulk PMMA (and PEO) where only the ideal glass temperature varies with composition and

$$T_{0,i}(\varphi_{eff}) = T_{0,i} + [T_{g,i}(\varphi_{eff}) - T_{g,i}] \quad (12)$$

where $T_{0,i}$ is the ideal glass temperature for homopolymers A or B and $T_{0,i}(\varphi_{eff})$ is the ideal glass temperature for each component in the blends. As noted in Figure 5, the model predictions with the above approximations are in sufficient agreement with the experimental $\tau(T)$, and this agreement improves in the case of the adjustable l_K (= 1.38 nm) (full quantitative agreement requires treating B_i and $\tau_{0,i}$ as adjustable parameters). The agreement further improves by allowing l_K to adjust for each blend composition. The result of this procedure is discussed later with respect to Figure 10. Here it suffices to mention that the self-concentration model adequately describes the PMMA segmental dynamics in the PMMA/PEO blends rich in PMMA.

Next we test the ability of the model to predict the PMMA segmental dynamics in the same blends but at elevated pressures. In Figure 6, the result of application of pressure to the PMMA segmental (α) and local processes (β) is shown for some blend compositions. Increasing pressure slows down the segmental and the local PMMA dynamics, but the effect is more pronounced for the former process. Thus, increasing pressure results in the effective separation of the dynamic processes under "isothermal" conditions. Notice the linearity of the log τ vs P with slopes giving an apparent activation volume[37,57,58]

$$\Delta V = RT\left(\frac{\partial \ln \tau}{\partial P}\right)_T \quad (13)$$

which is found to be T-independent for the local β-process and strongly T-dependent for the slower α-process. This is depicted in Figure 7, where the apparent activation volumes associated with the α- and β-processes in PMMA and in the PMMA/PEO blends with $\varphi_{PMMA} = 0.9$, 0.8, and 0.7 are plotted as a function of the temperature difference from the respective T_g. Notice that the value of the apparent activation volume for the segmental process reaches the MMA molecular volume ($V_{MMA} \sim 100$ cm^3/mol) at a temperature some 100 K above T_g.

To test the model predictions at elevated pressures, we proceed in the following way: from the $\tau(T)$ and $\tau(P)$ dependencies we can extract the pressure dependence of the glass temperature (defined at $\tau \sim 1$ s). This is shown in Figure 8 for bulk PMMA and the blends rich in PMMA. Both "isothermal" and "isobaric" data are included as well as *PVT* literature data for PMMA and two PMMA/PEO blends with $\varphi_{PMMA} = 0.9$ and 0.8. There is an excellent agreement of the $T_g(P)$ dependencies as obtained from literature *PVT*[24] and DS. The $T_g(P)$ dependence can be parametrized according to

$$T_g(P) = T_g(0)\left(1 + \frac{\mu}{\nu}P\right)^{1/\mu} \quad (14)$$

where $T_g(0)$ is the value of T_g at atmospheric pressure and ν and μ are constants with values 399.15 K, 1830 ± 100 MPa, and 3.4 for PMMA; 370.15 K, 1295 ± 20 MPa, and 3.4 for the blend with $\varphi_{PMMA} = 0.9$; 354.15 K, 1350 ± 10 MPa, and 3.4 for the blend with $\varphi_{PMMA} = 0.8$; 333.15 K, 1130 ± 30 MPa, and 3.4 for the blend with $\varphi_{PMMA} = 0.7$ (the exponent μ was kept fixed to its PMMA value). The extracted initial slopes (at $P = 0.1$ MPa) assume the following values for PMMA and the blends with $\varphi_{PMMA} = 0.9$, 0.8, and 0.7: $(dT_g/dP)_{P\to 0} = 0.22$, 0.29, 0.26, and 0.29 K/MPa, respectively. Notice that the pressure coefficients of T_g are not very different in blends rich in PMMA.

Using the above T_g(P) dependencies, we can construct the $T_g(\varphi_{PMMA})$ dependence of Figure 4 at elevated pressures. The result is shown in Figure 9 for pressures of 0.1, 100, and 200 MPa. The figure depicts the predictions of the usual Fox equation as well as the predictions of the self-concentration model using either a fixed Kuhn length ($l_K = 1.38$ nm, dashed lines) or using l_K as an adjustable parameter. It can be noted that an adjustable l_K provides an excellent description of the blend T_g at elevated pressures.

The dependence of the characteristic length scale on (i) the blend composition, extracted from the $\tau(T)$ dependencies at 0.1 MPa (Figure 5), and (ii) on pressure, extracted from the T_g-(φ_{PMMA}) dependence at elevated pressures (Figure 9), is depicted in Figure 10. The figure displays a weak dependence of the Kuhn length on blend composition, as expected by the LM model. At the same time it shows a weak dependence on pressure, for pressures up to 500 MPa (in the calculation the density is corrected for the effect of pressure,[24,25] whereas C_∞ was treated as pressure-independent).[60] The latter is also anticipated; increasing pressure should result in the shrinkage of all length scales (density effect). Despite the fact that the reduction is higher than the density effect, we believe that this is the result of the longer extrapolations involved in determining T_g ($\tau \sim 1$ s). Overall, we find that practically the same length that was used to describe the PMMA segmental dynamics in the blends at atmospheric pressure can be used to describe the same process at elevated pressures. This constitutes a critical test of the validity of the self-concentration model as proposed by LM.

Last, we comment on the effect of pressure on the critical temperature, T_c, for polymer−polymer demixing. It is known that T_c is affected by pressure, and this could interfere with the PMMA segmental dynamics investigated herein. In a recent study,[61] such pressure effects were investigated by employing the pressure dependence of the Flory χ parameter. Assuming (i) identical compressibilities for the two components, (ii) identical thermal expansion coefficients for the homopolymers and the blends, and (iii) χ independent of composition resulted

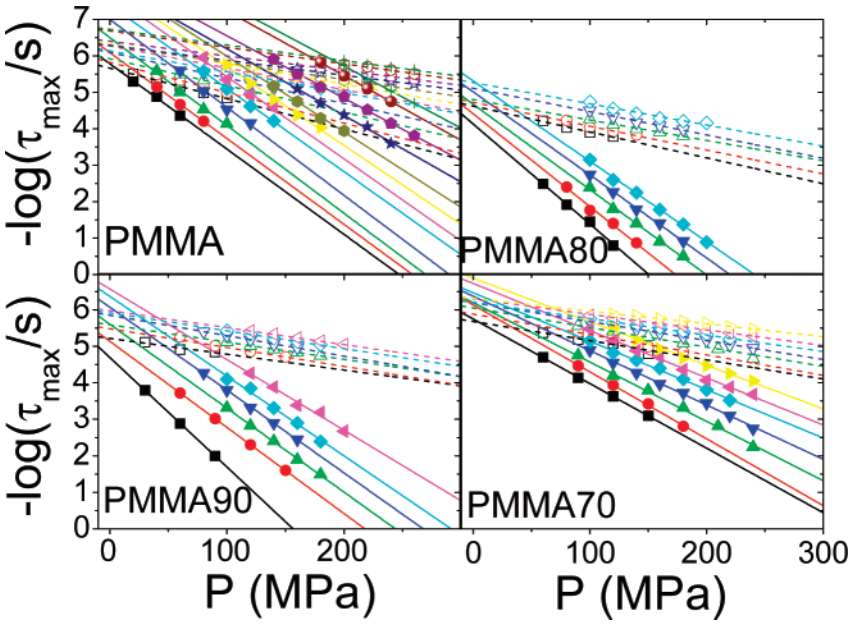

Figure 6. Pressure dependence of relaxation times corresponding to the segmental (filled symbols) and β-process (open symbols) of PMMA in the homopolymer and the PMMA/PEO blends rich in PMMA. The data points correspond to different "isotherms": PMMA: 436 < T < 491 K; PMMA/PEO (90/10): 413 < T < 443 K; PMMA/PEO (80/20): 388 < T < 408 K; PMMA/PEO (70/30): 436 < T < 491 K. The solid and dashed lines represent linear fits to the α- and β-processes, respectively.

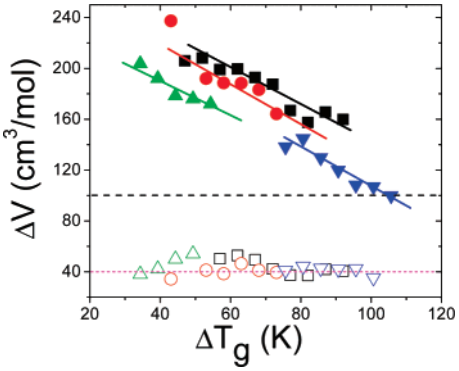

Figure 7. Apparent activation volumes as a function of the temperature difference from the respective T_g for bulk PMMA (squares) and in the PMMA/PEO blends with φ_{PMMA} = 0.9 (circles), φ_{PMMA} = 0.8 (up triangles), and φ_{PMMA} = 0.7 (down triangles). The filled and open symbols correspond to the α- and β-processes, respectively. Solid lines are guides to the eye. The dashed lines represent the volume of the PMMA (black) and PEO (red) repeat unit.

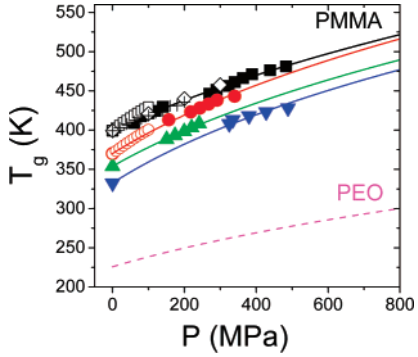

Figure 8. Pressure dependence of the glass temperature T_g of the PMMA homopolymer (black symbols) and the blends with φ_{PMMA} = 0.9 (circles), φ_{PMMA} = 0.8 (up triangles), and φ_{PMMA} = 0.7 (down triangles). The filled triangles are from DS. The open squares, open circles, and crosses are the results from *PVT* measurements.[24,25] The open rhombus are DS results from ref 59. The lines are fits to eq 14.

in the following approximate prediction for the pressure coefficient of the critical temperature:

$$\left(\frac{\partial T}{\partial P}\right)_c \sim \kappa_T T\left[\frac{\delta_{ip}}{\delta}\right]^2 \frac{1}{1-\beta T-\kappa_T P} \qquad (15)$$

where δ_{ip} is the internal pressure, δ is the solubility parameter, κ_T is the isothermal compressibility, and β is the coefficient of thermal expansion. Employing the representative values[61] $\delta/\delta_{ip} \sim 0.72$ and $\kappa_T = 2 \times 10^{-4}$ MPa^{-1}, $\beta = 4.5 \times 10^{-4}$ K^{-1} applicable to $\varphi_{PMMA} = 0.5$ and $T = 300$ K, we obtain $dT_c/dP \sim 0.15$ K/MPa. Since this pressure coefficient of T_c is smaller than the pressure coefficient of T_g for the PMMA-rich blends (from ~0.22 to 0.29 K/MPa), we conclude that the thermodynamic state of the blends remains unaffected by increasing pressure.

Comparison with Other Methods. To our knowledge, high-pressure measurements on the PMMA segmental dynamics in its blends with PEO do not exist. The only existing measurements are thermodynamic (*PVT*),[24,25] on the $T_g(P)$ at two blend compositions that are in excellent agreement with the dynamic DS results (Figure 9). Nevertheless, our results at $P = 0.1$ MPa can be compared with earlier neutron spin echo (NSE),[62] deuterium NMR,[31] and quasi-elastic neutron scattering (QENS)[29] reports.

The NSE measurements[62] were made on a perdeuterated PMMA/PEO blend with 0.7 < w_{PMMA} < 0.9 and for wave vectors in the range 0.35 < q < 1.66 Å^{-1}. However, τ_{NSE} were substantially shorter than the present τ_{DS} ($\tau_{NSE} \ll \tau_{DS}$), suggesting that NSE probed either the PMMA β-process or the faster PEO dynamics in the blends. The ^{2}H NMR experiments[31] were made for blends of PMMA with perdeuteriopoly(ethylene oxide) (d_4PEO) for concentrations in the range 0.05 < w_{PEO} < 0.3. The spin−lattice relaxation times were measured for temperatures in the range 300 < T < 475 K. Again, $\tau_{NMR} \ll \tau_{DS}$, suggesting that NMR probably were probing the PEO mobility in the blends. (The times were faster much beyond the expected $\tau_{NMR} = \tau_{DS}/3$, reflecting that NMR and DS probe respectively the second- and first-order Legendre polynomials.) Therefore, a direct comparison with the results of the present

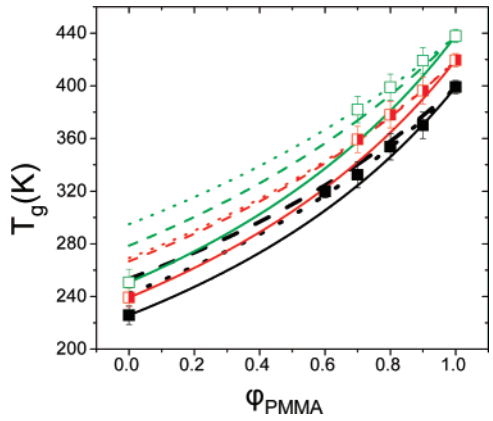

Figure 9. Glass temperatures obtained from DS and plotted vs φ_{PMMA}. Open symbols correspond to the data at 0.1 MPa, half-filled symbols to 100 MPa, and the open symbols to 200 MPa. The solid lines represent the Fox equation at the respective pressures. The dashed lines correspond to the self-concentration model predictions with no adjustable parameter. The dotted lines are fitted values to the self-concentration model using the Kuhn length as the only adjustable parameter.

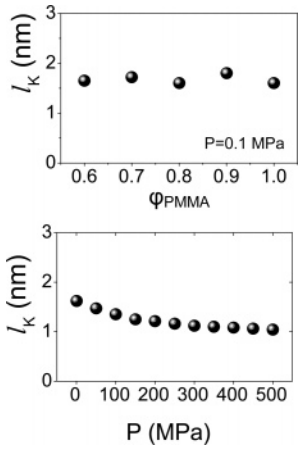

Figure 10. Composition dependence of l_K at $P = 0.1$ MPa (top) and pressure dependence of l_K extracted from the PMMA segmental dynamics in the PMMA-rich blends according to the predictions of the LM model (bottom).

investigation on the PMMA segmental dynamics cannot be made. The QENS experiments[29] were made on blends with deuterated PEO (hPMMA/dPEO) for concentrations $0.7 < w_{PMMA} < 1$ and for wave vectors in the range $0.6 < q < 1.7$ Å^{-1}. The much higher incoherent cross section of hydrogen with respect to that of deuterium guaranteed the probe of the PMMA segmental dynamics in the blends. Our DS results compare favorably with QENS (i.e., $\tau_{QENS} \sim \tau_{DS}$) especially at $q = 0.99$ Å^{-1}, i.e., a value located in the vicinity of the first structure factor maximum of PMMA. The erroneous conclusion, namely that $\varphi_S \sim 0$, stems from the smaller frequency range available to QENS and/or the much higher temperatures/extrapolations involved.

In addition to these reports on the segmental dynamics, there exist some efforts[6] to compare the terminal dynamics[1,63] in the PMMA/PEO system to the predictions of the LM model, however, with contradictory results on the model applicability (φ_S(PMMA) = 0 vs φ_S(PMMA) = 0.26).

Conclusion

The investigation of the segmental dynamics in a PMMA homopolymer revealed that intramolecular correlations have a dominant effect on the dynamics associated with the liquid-to-glass transition. On the basis of this finding, we employ the self-concentration model of Lodge and McLeish to describe the PMMA segmental dynamics in a series of PMMA/PEO blends rich in PMMA ($\varphi_{PMMA} \geq 0.6$). We find that the model adequately predicts the PMMA segmental dynamics in the blends. As a second step, we investigate the PMMA segmental dynamics in the same blends but at elevated pressures. This provides a critical test of the model as the self-concentration is not expected to change dramatically upon pressurization. It was found that pressure slows down the segmental dynamics and increases the respective glass temperatures but does not affect the length scale or the self-concentration associated with the dynamic glass transition, in agreement with the LM model. On the other hand, the model predictions for the PEO segmental dynamics could not be tested because of PEO crystallization at lower temperatures.

Acknowledgment. This work was supported by the Greek Secretariat for Research and Technology (GSRT) (PENED01/529 and PENED03/856) as well as by the Greek Ministry of Education through the PYTHAGORAS operational program.

References and Notes

(1) Colby, R. H. *Polymer* **1989**, *30*, 1275.
(2) Roovers, R. H.; Toporowski, P. M. *Macromolecules* **1992**, *25*, 1096.
(3) Chin, Y. H.; Zhang, C.; Wang, P.; Inglefield, P. T.; Jones, A. A.; Kambour, R. P.; Bendler, J. T.; White, D. M. *Macromolecules* **1992**, *25*, 3031.
(4) Roland, C. M.; Ngai, K. L. *Macromolecules* **1991**, *24*, 2261.
(5) Pathak, J. A.; Colby, R. H.; Floudas, G.; Jerome, R. *Macromolecules* **1999**, *32*, 2553.
(6) He, Y.; Lutz, T. R.; Ediger, M. D. *J. Chem. Phys.* **2003**, *119*, 9956.
(7) Krygier, E.; Lin, G.; Mendes, J.; Mukandela, G.; Azar, D.; Jones, A. A.; Pathak, J. A.; Colby, R. H.; Kumar, S. K.; Floudas, G.; Krishnamoutri, R.; Faust, R. *Macromolecules* **2005**, *38*, 7721.
(8) Floudas, G.; Steffen, W.; Fischer, E. W.; Brown, W. *J. Chem. Phys.* **1993**, *99*, 695.
(9) Floudas, G.; Fytas, G.; Brown, W. *J. Chem. Phys.* **1992**, *96*, 2164.
(10) Zetsche, A.; Fischer, E. W. *Acta Polym.* **1994**, *45*, 168.
(11) Lodge, T. P.; McLeish, T. C. B. *Macromolecules* **2000**, *33*, 5278.
(12) Chung, G.-C.; Kornfield, J. A.; Smith, S. D. *Macromolecules* **1994**, *27*, 964.
(13) Shenogin, S.; Kant, R.; Colby, R. H.; Kumar, S. K. *Macromolecules* **2007**, *40*, 5767.
(14) Kant, R.; Kumar, S. K.; Colby, R. H. *Macromolecules* **2003**, *36*, 10087.
(15) Kamath, S.; Colby, R. H.; Kumar, S. K.; Karatasos, K.; Floudas, G.; Fytas, G.; Roovers, J. E. L. *J. Chem. Phys.* **1999**, *111*, 6121.
(16) Kumar, S. K.; Colby, R. H.; Anastasiadis, S. H.; Fytas, G. *J. Chem. Phys.* **1996**, *105*, 3777.
(17) Cangialosi, D.; Alegria, A.; Colmenero, J. *Macromolecules* **2006**, *39*, 7149.
(18) Colby, R. H.; Lipson, J. E. G. *Macromolecules* **2005**, *38*, 4919.
(19) Lodge, T. P.; Wood, E. R.; Haley, J. C. *J. Polym. Sci., Polym. Phys.* **2006**, *44*, 756.
(20) Silva, G. G.; Machado, J. C.; Song, M.; Hourston, D. J. *J. Appl. Polym. Sci.* **2000**, *77*, 2034.
(21) Fernandes, A. C.; Barlow, J. W.; Paul, D. R. *J. Appl. Polym. Sci.* **1986**, *32*, 5481.
(22) Liberman, S. A.; Gomes, A. D. S.; Macchi, E. M. *J. Polym. Sci., Polym. Chem. Ed.* **1984**, *22*, 2809.
(23) Jin, X.; Zhang, S.; Runt, J. *Macromolecules* **2004**, *37*, 8110.
(24) Schmidt, M.; Maurer, F. H. J. *J. Polym. Sci., Part B: Polym. Phys.* **1998**, *36*, 1061.
(25) Zoller, P.; Walsh, D. *Pressure-Volume-Temperature Data for Polymers*; Technomic Publishing Co.: Lancaster, PA, 1995.
(26) Fytas, G.; Kanetakis, J.; Floudas, G.; Wang, C. H. *Polym. Commun.* **1990**, *31*, 437.
(27) Maranas, J. K. *Curr. Opin. Colloid Interface Sci.* **2007**, *12*, 29.
(28) Sakai, V. J.; Maranas, J. K.; Chowdhuri, Z.; Peral, I.; Copley, J. R. D. *J. Polym. Sci., Polym. Phys.* **2005**, *43*, 2914.
(29) Liu, J.; Sakai, V. J.; Maranas, J. K. *Macromolecules* **2006**, *39*, 2866.
(30) Genix, A.-C.; Arbe, A.; Alvarez, F.; Colmenero, J.; Willner, L.; Richter, D. *Phys. Rev. E* **2005**, *72*, 031808.
(31) Lutz, T. R.; He, Y.; Ediger, M. D.; Cao, H.; Lin, G.; Jones, A. A. *Macromolecules* **2003**, *36*, 1724.
(32) Haley, J. C.; Lodge, T. P. *J. Chem. Phys.* **2005**, *122*, 234914.

(33) Hopkinson, I.; Kiff, F. T.; Richards, R. W.; King, S. M.; Farren, T. *Polymer* **1995**, *36*, 3523.
(34) Ito, H.; Russell, T. P.; Wignall, G. D. *Macromolecules* **1987**, *20*, 2213.
(35) Cimmino, S.; Martuscelli, E.; Silvestre, C. *Polymer* **1989**, *30*, 393.
(36) Lefebvre, J. M.; Porter, R. S.; Wignall, G. D. *Polym. Eng. Sci.* **1987**, *27*, 433.
(37) Floudas, G. In *Broadband Dielectric Spectroscopy*; Kremer, F., Schönhals, A., Eds.; Springer: Berlin, 2002; Chapter 8.
(38) Havriliak, S.; Negami, S. *Polymer* **1967**, *8*, 161.
(39) Papadopoulos, P.; Peristeraki, D.; Floudas, G.; Koutalas, G.; Hadjichristidis, N. *Macromolecules* **2004**, *37*, 8116.
(40) Sokolov, A. P. *Science* **1996**, *273*, 1675.
(41) Angell, C. A. *Science* **1995**, *267*, 1924.
(42) Stillinger, F. H. *Science* **1995**, *267*, 1935.
(43) Ferry, J. D. *Viscoelastic Properties of Polymers*, 3rd ed.; Wiley: New York, 1980.
(44) Williams, G. *Trans. Faraday Soc.* **1966**, *62*, 2091.
(45) Ferrer, M.-L.; Lawrence, C.; Dermirjian, B. G.; Kivelson, D. *J. Chem. Phys.* **1998**, *109*, 8010.
(46) Roland, C. M.; Paluch, M.; Pakula, T.; Casalini, R. *Philos. Mag.* **2004**, *84*, 1573.
(47) Alba-Simionesco, C.; Cailliaux, A.; Tarjus, G. *Europhys. Lett.* **2004**, *68*, 58.
(48) Mpoukouvalas, K.; Floudas, G. *Phys. Rev. E* **2003**, *68*, 031801.
(49) Mpoukouvalas, K.; Gomopoulos, N.; Floudas, G.; Herrmann, C.; Hanewald, A.; Best, A. *Polymer* **2006**, *47*, 7170.
(50) Naoki, M.; Endou, H.; Matsumoto, K. *J. Phys. Chem.* **1987**, *91*, 4169.
(51) Floudas, G.; Mpoukouvalas, K.; Papadopoulos, P. *J. Chem. Phys.* **2006**, *124*, 074905.
(52) Casalini, R.; Roland, C. M.; Capaccioli, S. *J. Chem. Phys.* **2007**, *126*, 184903.
(53) Floudas, G.; Fytas, G.; Reisinger, T.; Wegner, G. *J. Chem. Phys.* **1999**, *111*, 9129.
(54) Mpoukouvalas, K.; Floudas, G.; Zhang, S. H.; Runt, J. *Macromolecules* **2005**, *38*, 552.
(55) Mpoukouvalas, K.; Floudas, G.; Verdock, B.; Du Prez, F. E. *Phys. Rev. E* **2005**, *72*, 011802.
(56) Fetters, L. J.; Lohse, D. J.; Richter, D.; Witten, T. A.; Zirkel, A. *Macromolecules* **1994**, *27*, 4639.
(57) Floudas, G.; Reisinger, T. *J. Chem. Phys.* **1999**, *111*, 5201.
(58) Floudas, G.; Gravalides, C.; Reisinger, T.; Wegner, G. *J. Chem. Phys.* **1999**, *111*, 9847.
(59) Theobald, S.; Pechwald, D.; Stoll, B. *Polymer* **2001**, *42*, 289.
(60) Tsolou, G.; Harmandaris, V. A.; Mavrantzas, V. G. *Makromol. Theory Simul.* **2006**, *15*, 381.
(61) Kumar, S. K. *Macromolecules* **2000**, *33*, 5285.
(62) Farago, B.; Chen, C.; Maranas, J. K.; Kamath, S.; Colby, R. H.; Pasquale, A. J.; Long, T. E. *Phys. Rev. E* **2005**, *72*, 031809.
(63) Zawada, J. A.; Ylitalo, C. M.; Fuller, G. G.; Colby, R. H.; Long, T. E. *Macromolecules* **1992**, *25*, 2896.

MA702299N